Computational Study on Unsteady Mechanism of Spinning Detonations

Akiko Matsuo*, and Yuta Sugiyama*

* Department of Mechanical Engineering, Keio University, Kanagawa, Japan
(Tel : +81-45-563-1141; E-mail: matsuo@mech.keio.ac.jp)

Abstract: Spinning detonations propagating in a circular tube were numerically investigated with a one-step irreversible reaction model governed by Arrhenius kinetics. Activation energy is used as parameter as 10, 20, 27 and 35, and the specific heat ratio and the heat release are fixed as 1.2 and 50. The time evolution of the simulation results was utilized to reveal the propagation mechanism of single-headed spinning detonation. The track angle of soot record on the tube wall was numerically reproduced with various levels of activation energy, and the simulated unique angle was the same as that of the previous reports. The maximum pressure histories of the shock front on the tube wall showed stable pitch at Ea=10, periodical unstable pitch at Ea=20 and 27 and unstable pitch consisting of stable, periodical unstable and weak modes at Ea=35, respectively. In the weak mode, there is no Mach leg on the shock front, where the pressure level is much lower than the other modes. The shock front shapes and the pressure profiles on the tube wall clarified the mechanisms of these stable and unstable modes. In the stable pitch at Ea=10, the maximum pressure history on the tube wall remained nearly constant, and the steady single Mach leg on the shock front rotated at a constant speed. The high and low frequency pressure oscillations appeared in the periodical unstable pitch at Ea=20 and 27 of the maximum pressure history. The high frequency was one cycle of a self-induced oscillation by generation and decay in complex Mach interaction due to the variation in intensity of the transverse wave behind the shock front. Eventually, sequential high frequency oscillations formed the low frequency behavior because the frequency behavior was not always the same for each cycle. In unstable pitch at Ea=35, there are stable, periodical unstable and weak modes in one cycle of the low frequency oscillation in the maximum pressure history, and the pressure amplitude of low frequency was much larger than the others. The pressure peak appeared after weak mode, and the stable, periodical unstable and weak modes were sequentially observed with pressure decay. A series of simulations of spinning detonations clarified that the unsteady mechanism behind the shock front depending on the activation energy.

Keywords: Spinning Detonation, Propagation Mechanism, Activation Energy, Unstable Pitch

1. INTRODUCTION

Detonations are supersonic flow phenomena with leading shock waves that ignite premixed gas. The structure and properties of detonation have been investigated by many researchers using experimental, theoretical, and numerical approaches. Although detonation has been experimentally shown to propagate in both longitudinal and transverse directions with unstable three-dimensional structure, the detailed three-dimensional structure of detonation has not been become clear because of difficulty of three-dimensional visualization by experimental devices.

Shock structure of detonation is composed of incident shock, Mach stem and transverse waves which propagate perpendicularly to the shock front. A few modes have been observed in detonation of circular tube such as spinning (single-headed), two-headed and multi-headed mode, and they are classified according to the number of transverse wave. Spinning detonation in circular tube, discovered experimentally in 1926 by Campbell and Woodhead[1–3], is observed near detonation limit and the lowest mode that has only one transverse wave in a circumference direction, whereas two-headed detonation has two transverse waves along circumference and one transverse wave along a radius. The spinning detonation propagates helically on the wall and rotates around the tube axis. It is also reported that the mean propagating velocity of spinning detonation is about 0.8 - $0.9D_{CJ}$ (D_{CJ}: CJ detonation velocity). A theoretical study by Fay[4] showed that the ratio of spin pitch to the tube diameter, 3.13, was derived from an acoustic theory. The acoustic theory can explain the property of spinning detonation but cannot explain its structure. Schott[5] tried to understand the shock structure of spinning detonation, and they concluded that the wave front contains a complex Mach interaction. Voitekhovskii[6] and his co-workers measured the Mach configuration by examining smoked disks attached to the end plate of the detonation tube. Their experimental observation says that it consists of a “leg” and one or two “whiskers.” They also used the term “leg” as in “Mach leg.” Topchian and Ul’yanitskii[7] investigated the instability of the spinning detonation and found three different types of pitch mode; stable pitch, periodical unstable pitch, and pitch covered with a cellular pattern.

Many researchers have numerically studied three-dimensional propagation of detonation wave. Williams et al.[8] studied the two-headed mode, and Deledicque and Papalexandris[9] studied multi-headed mode in a rectangular tube using a one-step chemical reaction model of Arrhenius' form. Eto et al.[10] and Tsuboi et al.[11] investigated the detailed shock structures in rectangular tube of single- and two-headed modes using detailed reaction model. Tsuboi et al.[12, 13] and Virot et al.[14] investigated the spinning detonation in a circular tube, and their simulated results agreed well with experimental data.

The aim of this work is to clarify the propagation mechanism of spinning detonation in a circular tube by three-dimensional numerical simulations changing activation energy. The detailed discussion is carried out to explain the unsteady propagation mechanism with the time evolution of the simulated results.

2. PHYSICAL MODEL AND NUMERICAL METHOD

The governing equations are the compressible and reactive three-dimensional Euler equations. The fluid is an ideal gas with constant specific heat ratio, and all diffusive are neglected. Chemistry is modeled by a one-step Arrhenius kinetics whose parameters are specific heat ratio, heat release and activation energy[15]. As discretization methods, Yee’s Non-MUSCL Type 2nd-Order Upwind Scheme[16] is used for the spatial integration, and Point-Implicit Method that treats only source term implicitly is used for the time integration. Governing equations are normalized by values of standard region and half-reaction length, $L_{1/2}$, which is the distance required for mass fraction of reactant reducing to 0.5 in

one-dimensional steady CJ detonation analysis. Grid resolution is defined as the number of grid points in half-reaction length. In our simulations, heat release, degree of overdrive (D^2/D^2_{CJ}: D is detonation velocity) and specific heat ratio are fixed as 50, 1.0, 1.2, respectively and activation energy is chosen as a parameter.

The computational grid is a cylindrical system, whose diameter is fixed as $3.51L_{1/2}$, with 451×43×205 for axial, radial and circumferential directions, respectively. A high grid resolution in circumferential direction, where at least 20 grid points in half reaction length are set on the tube wall, is needed because the spinning detonation has a transverse detonation on the tube wall. The axial length in the computational grid is more than $70L_{1/2}$ to avoid disturbance from the outflow boundary, where values are extrapolated with zero-gradient condition. The present computational grid has a singular point in the tube center, where physical values are an average around it. The results of one-dimensional steady simulation are used as an initial condition. Sheets of three-dimensional unburned gas mixture behind detonation front are artificially added in order to create initial three-dimensional disturbances.

3. RESULT AND DISCUSSION

3.1 track angle and maximum pressure histories of shock front

The soot tracks on the tube wall were recorded in previous experimental studies. A track angle, which is defined as arctangent of the pitch of the spin divided by length in circumference, is derived from the experimental observation. The track angle is about 45 degrees under various operating conditions, and the value is also derived by an acoustic theory[4].

Figure 1 shows the maximum pressure histories on the tube wall in the cases of activation energy (a) Ea=10, (b) Ea=20 and (c) Ea=27, respectively. The trajectories of the darker region correspond to the soot track in the experiments, and therefore α in Fig. 1 is the track angle. In our simulations, the track angle is about 43 degrees regardless of the activation energy, which agrees well with the previous experimental[6] and numerical studies[13]. Consequently, we confirmed that the present simulations could reproduce the basic characteristics of spinning detonation. Additionally, Fig. 1a shows stable dark belt as high pressure region, but there is unstable behavior in Fig. 1b and 1c. This feature agrees with the experimental observation of uniform and irregular spin modes by Schott[5] and denotes that an increase of activation energy makes the simulated spinning detonation unstable.

Figure 2 shows the maximum pressure histories of the shock front on the tube wall at (a) Ea=10, (b) Ea=20 and (c) Ea=27, respectively. Pressures are normalized by von Neumann spike of CJ condition of one-dimensional steady simulation, P_{vN}=42.06. White plots denote an average pressure, which is obtained from one cycle of the high frequency oscillation in the simulated data. In all the simulation results, the spinning detonation appears, and the period of spinning detonation traveling around the tube wall is about 2 of the normalized time. The pressure remains constant with negligibly small amplitude of oscillation at Ea=10 in Fig. 2a, and the representative value of the normalized steady pressure of spinning detonation, Pss/P_{vN}, is estimated as 1.66. This stable behavior agrees with the trajectory of the maximum pressure history on the tube wall in Fig. 1a.

Meanwhile, the high frequency pressure oscillations with large amplitude appear in Figs. 2b and 2c, and the periods are much less than the period of spinning detonation traveling around the tube wall. Figures 2b and 2c also show the low frequency oscillations in the average pressure of white plots, and these low frequency periods are about 15 of the normalized time. In Fig. 2b, the average pressure plots slightly oscillate. As the activation energy increases from Ea=20 to 27, the amplitude of low frequency oscillation becomes larger, which is known as the basic characteristics of detonation propagation. He and Stewart[17] reported the critical activation energy, 25.3, based on the stability analysis of one-dimensional detonation, where the shock pressure history oscillates when the activation energy is greater than the critical value. Since the oscillations appear at Ea=20 in the present simulations, the criterion on stability is not applicable to spinning detonation.

3.2 Shock structure

3.2.1 Stable pitch at Ea=10

The shock structure of stable pitch is investigated in detail using the simulated result at Ea=10. Figures 3 and 4 show the shock front shapes viewed from the front side and instantaneous pressure distribution at the shock front on the tube wall, respectively, and the moments of ‘a’ to ‘c’ in Fig. 4 correspond to Figs. 3a to 3c. As observed in Fig. 3, the shock front remains the same shape and rotates at a constant speed in clockwise direction. Mach leg always stands orthogonal to the tube wall, and no other waves are generated in the shock front. The pressure profiles in Fig. 4 are identical and just shift from left to right.

Figure 5 shows (a) pressure and (b) reactant mass fraction distributions on the tube wall at a certain moment, and the distribution in reactant mass fraction almost corresponds to that in temperature. The distributions on the tube wall always show a unique profile and move upward at a constant speed. The high pressure region behind the transverse wave, which is not coupled with the exothermic region, in Fig. 5a makes the trajectories of the stable dark belt in Fig. 1a. Here, the transverse wave behind the Mach leg is not the transverse detonation. In the previous experimental[5] and numerical studies[13], the transverse wave is always the detonation wave. This fundamental difference comes from the reaction model used in the present study.

The simulated longitudinal velocity of spinning detonation is $0.89D_{CJ}$, as well as the experimental observations. Mach numbers in longitudinal and circumferential directions are 5.53 and 5.07, and the resultant Mach number, $(M_{tran})_{c/l}$, and the track angle are derived as 7.50 and 43 degrees. Meanwhile, Mach number, $(M_{tran})_{flow}$, derived from pressure behind the transverse wave in Fig. 5a ($P_{tran}=1.57P_{vN}$) is 7.79, which, as a matter of course, is consistent with $(M_{tran})_{c/l}$.

3.2.2 Periodical unstable pitch at Ea=20 and 27

The shock structure of unstable pitch in Fig. 1b is discussed using the simulated results of Ea=27, whose unsteady mechanism is essentially the same as the other cases showing high and low frequency oscillations. Figure 6 is the time evolution of shock front shapes with schematic pictures explaining the shock structure viewed from the front side. Figures 7 and 8 show the detailed pressure histories between time 90 and 92, which is the period that spinning detonation travels around the tube wall, and the instantaneous pressure distributions at the shock front on the tube wall, respectively. Black circles in Fig. 8 indicate the pressure of Mach leg. The moments of ‘a’ to ‘h’ in Fig. 6 corresponds to denotation of Figs. 7 and 8. A sequence in Figs. 6 and 8 schematically and quantitatively shows the generation and decay of complex

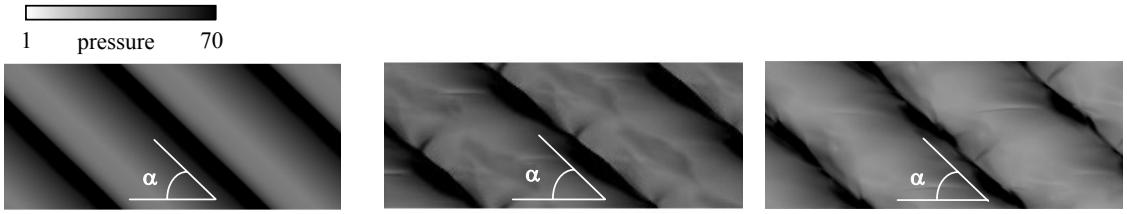

(a) Ea=10 (b) Ea=20 (b) Ea=27

Fig. 1 Numerical soot track images using maximum pressure histories on the tube wall, (a) Ea=10 (b) Ea=20 and (c) Ea=27.

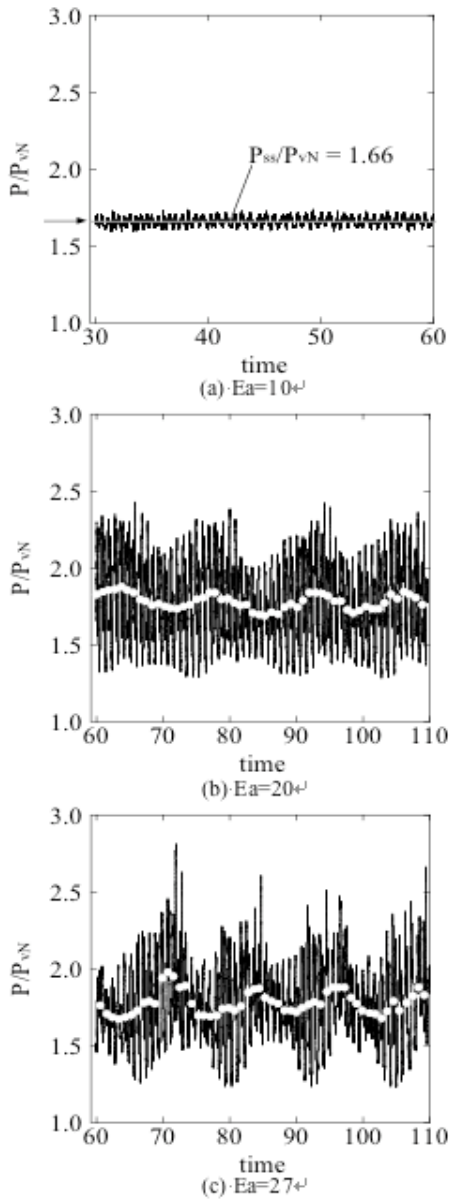

Fig. 2 Maximum pressure histories of the shock front on the tube wall, (a) Ea=10, (b) Ea=20 and (c) Ea=27.

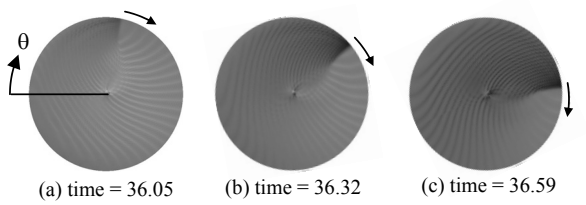

Fig. 3 Time evolution of shock front shapes viewed from the front side at Ea=10.

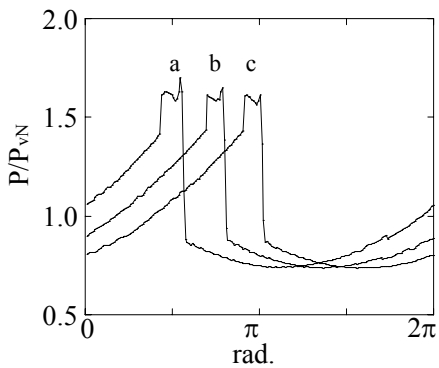

Fig. 4 Instantaneous pressure distributions at the shock front on the tube wall at Ea=10.

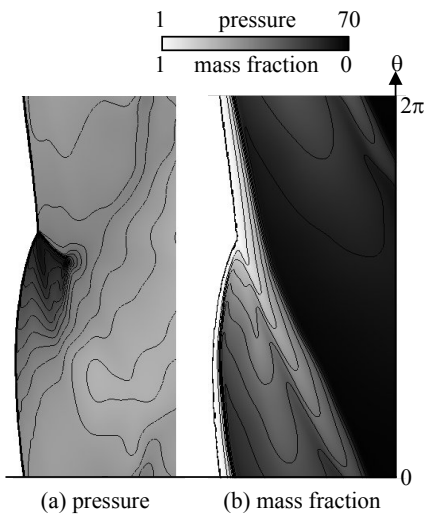

Fig. 5 Instantaneous distributions on the tube wall, (a) pressure and (b) reactant mass fraction at Ea=10.

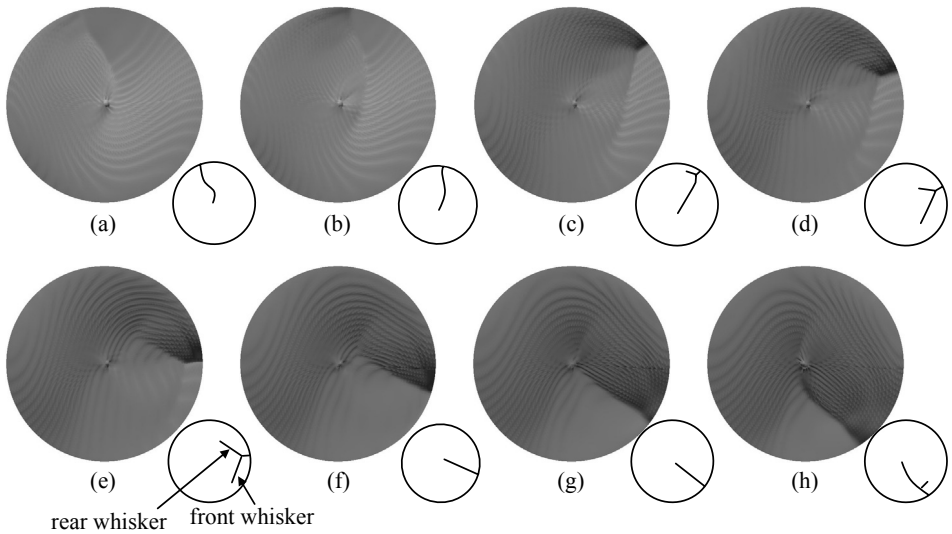

Fig. 6 Time evolution of shock front shapes with schematic pictures explaining the shock structure viewed from the front side at Ea=27.

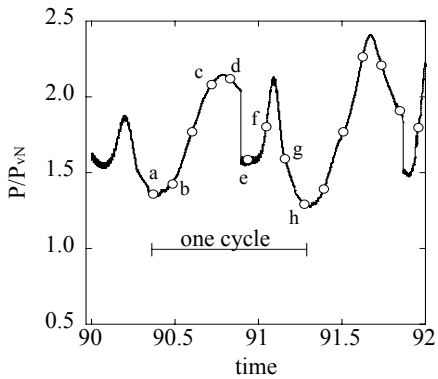

Fig. 7 Maximum pressure history of the shock front on the tube wall at Ea=27.

Mach interaction. In Fig. 8, the profile 'a' is almost the same as the profile 'h', and therefore the moment 'h' is the beginning of a new cycle. Additionally, Fig. 7 indicates that it takes about 1 of the normalized time to complete one cycle, and the intensity of pressure varies periodically with two peaks during the cycle.

A series of events is explained using Figs. 6-8, as follows with denotation in figures. (a) Mach leg stands orthogonal to the wall. The maximum pressure of the shock front is nearly lowest of the cycle, and the pressure jumps up at the Mach leg and gradually decreases behind the jump. (b) The Mach leg rotates keeping the shock front shape and shock strength, and the pressure profile in Fig. 8 is similar to that in Fig. 4. (c) The front and rear whiskers are generated on the shock front, and the maximum pressure behind the Mach leg increases during the propagation. (d) The Mach leg rotates keeping the shock structure of 'c'. The highest pressure in the cycle is obtained, which is located in the second jump behind the first jump of the Mach leg. (e) The shock structure is the same as that of 'c' and 'd', but the front whisker is close to the tube wall. The maximum pressure becomes lower because the second jump vanishes behind the Mach leg. (f) The whiskers disappear in the shock structure because the front whisker hits on the tube wall. Consequently, the pressure behind the Mach leg becomes stronger due to the hit. (g, h) The Mach leg rotates keeping the shock front shape, and the maximum pressure decreases to the lowest pressure in the cycle. A new cycle starts again at 'h'. Focus on the behavior of black circles in Fig. 8, pressure on Mach leg oscillates around the Pss except at the moment 'f'. This indicates that averaged velocity of Mach leg is the same as that in the case of Ea=10.

The maximum pressure gradually increases from 'a' to 'd', and the second jump appears behind the first jump in 'c' and 'd' in Fig. 8. The first jump indicates the triple point at the transverse wave, and the second jump means the decoupling of the shock wave and reaction region. The pressure of the second jump suddenly drops down from 'd' to 'e'. In order to clarify the above feature, the time evolution of distribution of (a) pressure and (b) reactant mass fraction on the tube wall is shown in Fig. 9. The denotation in Fig. 9 corresponds to that in Figs. 6-8. The pressure behind the transverse wave at 'c' in Fig. 9a is much higher than that at 'a', as well as the profiles in Fig. 8. At 'a' in Fig. 9b, the unburned region in front of the transverse wave is wider than the other. Then, the transverse wave is accelerated there and eventually arrives at the end of the wider unburned region at 'e', where the reactant is not consumed fully. The rest of reactant exists at regular intervals in Fig. 9b. Figure 9 says that the transverse wave consumes the unburned gas behind the incident shock, and the consumption rate depends on the intensity of the transverse wave due to the path width of the unburned region. The resulting inhomogeneous distribution of reactant mass fraction behind the Mach stem disappears due to the progress of the chemical reaction.

It is concluded that the mechanism of the generation and decay of complex Mach interaction makes the high frequency oscillation in the maximum pressure history on the shock front. The oscillation is the self-induced one depending on the intensity of the transverse wave. The shape of unburned region behind the incident shock is not always the same as observed in Fig. 9, because it depends on the behavior of the former transverse wave. Consequently, the low frequency oscillation appears in the pressure histories in Figs. 2b and 2c.

As for the track angle, the simulated longitudinal velocity

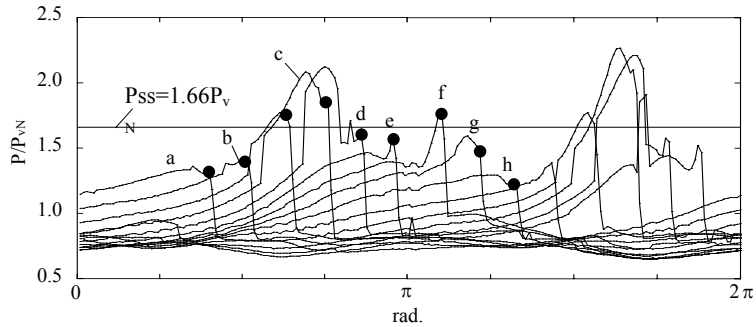

Fig. 8 Instantaneous pressure distributions at the shock front on the tube wall at Ea=27. Black circles indicate the pressure of Mach leg.

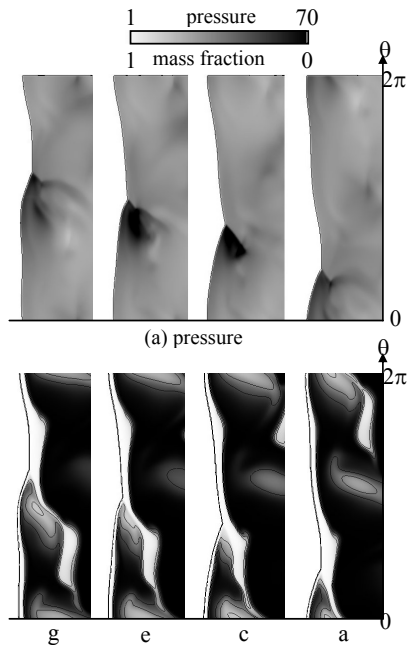

Fig. 9 Time evolution of distributions on the tube wall, (a) pressure and (b) reactant mass fraction at Ea=27.

of spinning detonation is 0.85-0.93D_{CJ} depending on the time. Mach numbers in longitudinal and circumferential directions are 5.26-5.75 and 5.07, and the resultant Mach number, $(M_{tran})_{c/l}$, and the track angle are derived as 7.31-7.67 and 41-44 degrees in one cycle of high-frequency oscillation. The average track angle of simulated track angle is 43 degrees and agrees with that of Ea=10, and experimental observations.

3.2.2 Unstable Pitch at Ea=35

Figure 11 shows the maximum pressure profile on the wall at Ea=35. Pressures are normalized by von Neumann spike of CJ condition of one-dimensional steady simulation, P_{vN}=42.06.

White plots denote an average pressure, which is obtained from one cycle of the high frequency oscillation in the simulated data, and low frequency oscillation appeares. Compared with the maximum pressure history on the wall at Ea=20 and 27 as shown Fig. 2b and 2c, the amplitude of low frequency oscillation at Ea=35 is larger and there are sudden pressure jumps, which are similar to reignition of unsteady one-dimensional detonation[15]. Figure 12 denotes the numerical soot track images using maximum pressure histories on the tube wall and the close up view of Fig. 11 with maximum pressure history on the wall. Figures 12a and 12b show one cycle of low frequency oscillation, respectively. There are high frequency oscillations, where the average pressure is larger than Pss, and the maximum pressure history shows the periodical unstable pitch, with the track angle of about 43 degrees. Meanwhile, when the average pressure is lower than Pss, the track angle is about 37 degrees, which is lower than that at experimental observation[5]. In this weak pitch, Mach leg disappears on the wall. At time=96.3, the average pressure suddenly increases and Mach leg appears. After pressure increases, the average pressure becomes much higher than Pss with track angle of 46 degrees, and stable pitch appears on the maximum pressure history on the wall at 98<time<103. In case of Ea=35, there are stable, periodical unstable and weak modes in one cycle of the low frequency oscillation in the maximum pressure history.

Figure 13 shows the typical detonation fronts viewed from the front side at (a) time=79.6, (b) time=99.0 and (c) time=95.85. At Fig. 13a, there exists complex Mach interaction with one Mach leg and two whiskers, which is one of the characteristics of periodical unstable pitch. At Fig. 13b, there are one Mach leg and one whisker of stable pitch, where the Mach leg rotates in clockwise direction. At Fig. 13c, Mach leg does not exist clearly by the decrease of averaged pressure as shown Fig. 12b.

4. CONCLUSION

Spinning detonations with various levels of activation energy, Ea=10, 20, 27 and 35 were numerically investigated using three-dimensional Euler equations with a one-step chemical reaction model governed by Arrhenius kinetics. The track angle was numerically measured using the maximum pressure history on the tube wall, which was about 43 degrees regardless of activation energy. The track angle was almost the same as that of past experimental and numerical studies. The simulated results showed that three kinds of spin modes on the shock front structure depending on the activation energy; the first was the stable pitch at Ea=10, the second was the periodical unstable pitch at Ea=20 and 27, and the third was the unstable pitch observed at Ea=35. At the lower

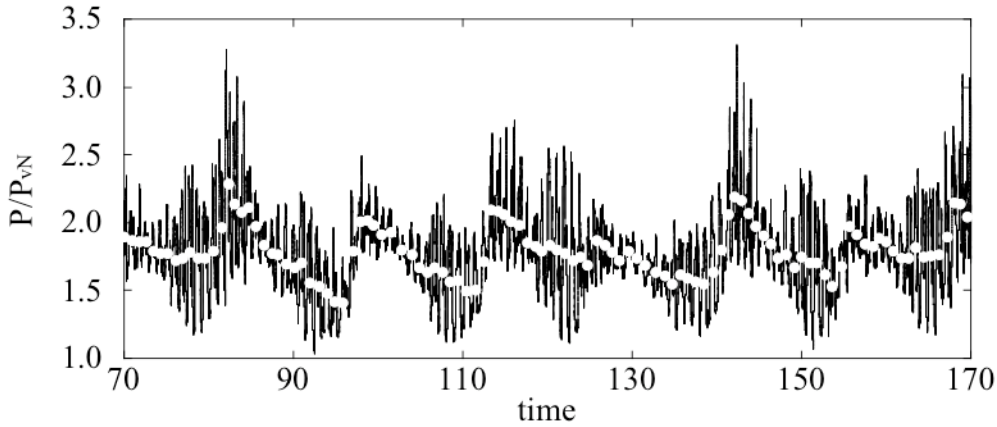

Fig. 11 Maximum pressure histories of the shock front on the tube wall, at Ea=35

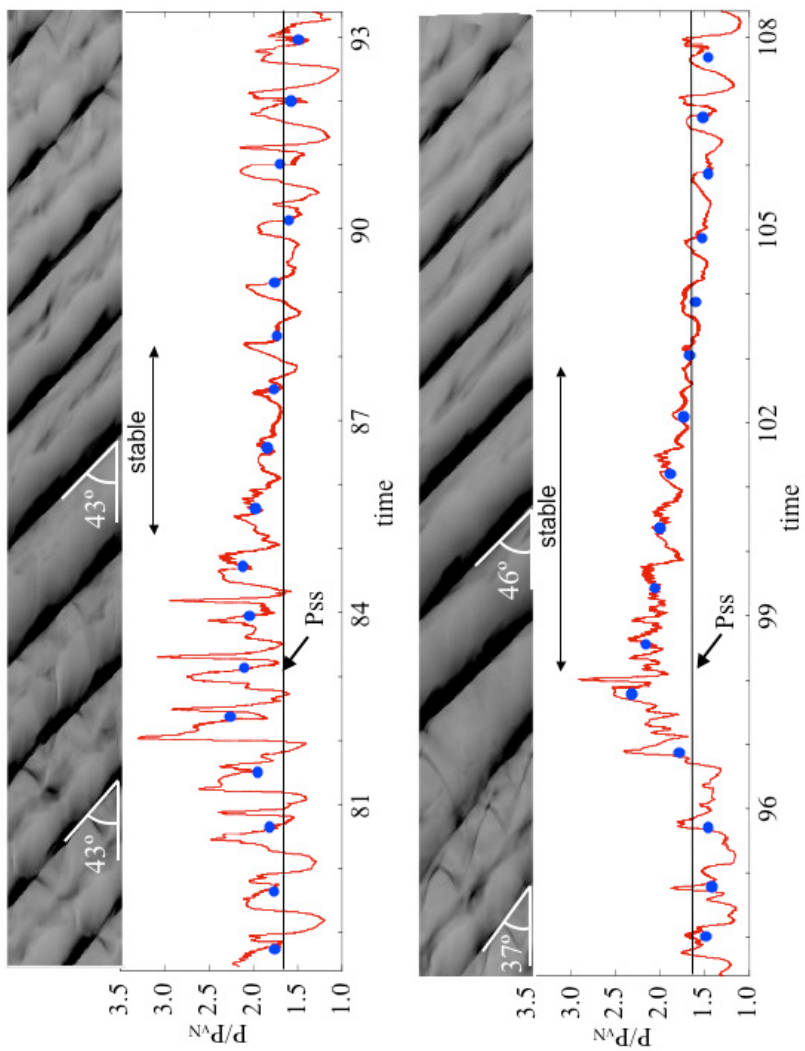

(a) 78.4<time<93.5 (b) 93.5<time<109

Fig. 12 Maximum pressure history on the wall at Ea=35 and close up view of Fig. 11 (a) 78.4<t<93.5 (b) 93.5<t<109

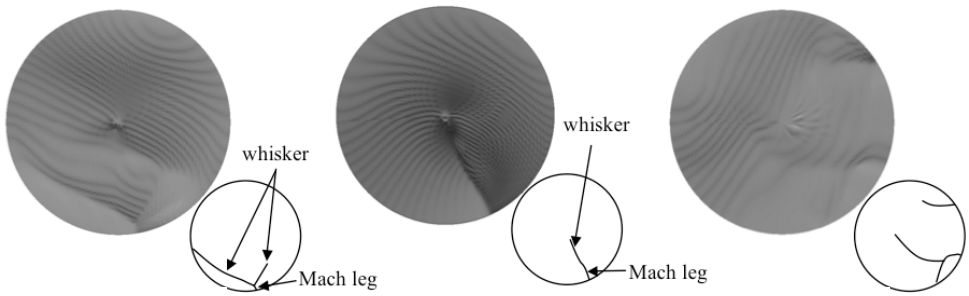

Fig. 13 Detonation fronts viewed from the front side at (a) time=79.63, (b) 99.10 and (c) 95.85

activation energy at Ea=10, the maximum pressure history of the shock front on the tube wall remained nearly constant, and the single Mach leg always existed on the shock front and rotated at the constant speed. Meanwhile, at the higher activation energy of Ea=20 and 27, the high and low frequency oscillations appeared in the maximum pressure histories. The generation and decay of complex Mach interaction occurred on the shock front sequentially and caused the high frequency oscillation. The sequence of events for the generation and decay having two pressure peaks in one cycle was clarified in detail using the time evolution of the simulated data. The high frequency oscillation was caused by the self-induced mechanism for the complex Mach interaction depending on the intensity of the transverse wave, which consumed the unburned gas behind the incident shock. Additionally, the shape of unburned region was not always the same for each cycle. Therefore, the low frequency oscillation appeared due to the change of intensity of the self-induced oscillation. In unstable pitch at Ea=35, there were stable, periodical unstable and weak modes in one cycle of the low frequency oscillation in the maximum pressure history, and the pressure amplitude of low frequency was much larger than the others. The pressure peak appeared after weak mode, and the stable, periodical unstable and weak modes were sequentially observed with pressure decay. A series of simulations of spinning detonations clarified that the unsteady mechanism behind the shock front depending on the activation energy.

REFERENCES

[1] 1926, Campbell, C., Woodhead, D.W., *J. Chem. Soc*. pp.3010-3021.
[2] 1927, Campbell, C., Woodhead, D.W., *J. Chem. Soc*. pp.1572-1578..
[3] 1928, Campbell, C., Finch, A.C., *J. Chem. Soc*. pp.2094-2106.
[4] 1952, Fay, J.A., *J. Chem. Phys*, Vol.20, pp.942-950.
[5] 1965, Schott, G.L., *Phys. Fluids*, Vol.8, pp.850-865.
[6] 1963, Voitsekhovskii, B.V., Mitrofanov, V. V. and Topchian, M.E., Sibirsk, Izd-vo, Odetl. Adak. Nauk SSR, Novosibirsk, Translation 1966, *Wright-Patterson Air Force Base Report*, FTD-MT-64-527 (AD-633-821).
[7] 1976, Topchian, M.E. and Ul'yanitskii, V.Y., *Acta Astronaut*, Vol.3, pp.771-779.
[8] 1996, Williams, D.N., Bauwens, L. and Oran, E.S., Proc. *Combust. Inst*. Vol.26, pp.2991-2998.
[9] 2006, Deledicque, V., Papalexandris, M.V., *Combust. Flame*, Vol.144, pp.821-837.
[10] 2005, Eto, K., Tsuboi, N. and Hayashi, A.K., *Proc. Combust. Inst*, Vol.30, pp.1907-1913.
[11] 2002, Tsuboi, N., Katoh, S. and Hayashi, A.K., *Proc. Combust. Inst*, Vol.29, pp.2783-2788.
[12] 2007, Tsuboi, N. and Hayashi, A. K., *Proc. Combust. Inst*. Vol.31, pp.2389-2396.
[13] 2007, Tsuboi, N., Eto, K. and Hayashi, A.K., *Combust. Flame*, Vol.149, pp.144-161.
[14] 2007, Virot, F., Khasainov, B., Desbordes, D. and Presles, H., *21st International Colloquium on the Dynamics of Explosions and Reactive Systems on CD-ROM.*
[15] 2003, Daimon, Y. and Matsuo, A., *Phys. Fluids* Vol. 15 pp.112-122.
[16] 1987, Yee, H.C., *NASA Technical Memorandum* 89464.
[17] 1990, Lee, H.I. and Stewart, D.S., *J. Fluid Mech*., vol.216, pp.103-132.